Environment. Technology. Resources. Rezekne, Latvia
Proceedings of the 14th International Scientific and Practical Conference. Volume 3, 282-288

Researching the Process of Laser Structuring of the Surface of Aluminum

Kevins Bulavskis
Engineering Faculty
Rezekne Academy of Technologies
Rezekne, Latvia
k26bulavskis@gmail.com

Emil Yankov
Engineering Faculty
Rezekne Academy of Technologies
Rezekne, Latvia
emil.yankov@rta.lv

Lyubomir Lazov
Engineering Faculty
Rezekne Academy of Technologies
Rezekne, Latvia
Lyubomir.Lazov@rta.lv

Antons Pacejs
Engineering Faculty
Rezekne Academy of Technologies
Rezekne, Latvia
antons.pacejs@rta.lv

***Abstract*. In this scientific study, the ability to modify the surface using nanosecond 1064 nm fiber laser by controlling the speed and scanning line step in the marking process was demonstrated. An experimental matrix for laser marking was developed, consisting of 8 columns for marking line step and 5 rows for marking speed. The laser marked surfaces were measured using a laser scanning microscope and compared with the surface as supplied. From the obtained deviations of roughness Ra, Rz and Rq as a function of marking speed and marking line step, graphical dependencies were constructed for comparative analysis. The modified roughness is also compared with the roughness as supplied. Within this research the effect of laser treatment on the hydrophilicity/hydrophobicity of the surface was studied as well. Plots of dependences of the contact angle CA, the marking line step Δx and the overlap coefficient K_{soc} are plotted.**

Keywords: laser marking, aluminum, laser texturing, laser structuring, roughness, hydrophobia.

I INTRODUCTION

Aluminum alloys are an important engineering material in the automobile, rail, and aerospace industries as the overall performance meets the requirements of mechanical strength and low weight as well as due to their low density and high specific strength [1]. The surface quality is quite important for the efficient working of machine parts. The structure of a machined surface is one of the most important criteria in terms of quality, and tribological properties of the machined surface. Generally, the surface quality is characterized with surface roughness. When using various kinds of solid materials, the roughness of the surface has a significant effect on their properties. Surface roughness is one of the most important characteristics of materials and affects wear resistance, contact rigidity, corrosion resistance and other functional characteristics of the surface [2]. Many approaches for increasing surface roughness have been studied over recent decades. For example, chemical etching, electrochemical etching (ECM), and laser surface texturing (LST). Among these methods, LST owns several advantages. First of all, chemical and ECM etching processes are accompanied by chemical work, which adversely affects the environment. Also, in comparison to LST, chemical etching consumes more processing time while ECM is limited to electrically conductive materials only and so LST is regarded as a more efficient, precise, and versatile approach to increase surface roughness [3]. This issue makes it necessary to study the process of laser structuring or texturing, assuming a series of experiments with varying parameters. To achieve a successful combination in the joining of dissimilar types of materials is imperative in creating a solid bond and, because the interactions take place on material surfaces, a tool or procedure for creating the bond is needed, and Laser Surface Texturing (LST) offers the perfect outcome.

Print ISSN 1691-5402
Online ISSN 2256-070X
https://doi.org/10.17770/etr2023vol3.7271

Enhancing fundamental characters, such as sustainability, tribological and biocompatibility, LST offers precise control regarding the main parameters of the characterization of microstructures (shape, roughness, width, depth, size, recast material, etc.) Laser surface texturing (LST) is a method to engender patterns on the surface of materials to accomplish microstructures. LST can remove the material from the surface (by dissolution, evaporation, expulsion and/or melting) to improve joining properties [4]. In addition, laser surface microstructuring has a number of advantages: high efficiency, good controllability, environmental friendly nature, and the capability of fabricating surface texture with high complexity and accuracy [5]. And also, special studies involve studying the possibility of the influence of laser structuring on hydrophilicity and hydrophobicity. In recent years, the wettability of material surface has been widely concerned, especially super-hydrophilic and super-hydrophobic [6].

Hydrophilic materials have potential for use in environmental purification, outdoor protection, medical and health, agriculture, food packaging and other fields [7].

Superhydrophobic surfaces are extremely hard to wet (low surface wettability), and such surfaces with this distinctive characteristic are found in nature. These surfaces have water contact angles greater than 150º and small roll-off angles less than 10º [12].

Wettability can be measured by water droplet contact angle (CA). CA is the angle between the surface of the liquid and the outline of the contact surface (solid surface typically). When the CA is less than 90°, the surface is hydrophilic; when the CA is greater than 90°, the surface is hydrophobic [6] [7].

There are two main factors affect the wettability of the material surface including surface roughness and surface energy, in which roughness is generally considered to be the key factor. At present, the preparation methods of super-hydrophilic and super-hydrophobic materials mainly focus on the surface roughness of the structural materials. Therefore, the micro/nanoarray structure is the key factor to make materials super hydrophilic or hydrophobic. There are several ways to fabricate the hybrid micro/nano structure on the materials, including sol-gel method, chemical vapor deposition, chemical etching, nanoimprint lithography, electrode position, self-assembly, laser fabricate, and more. Laser as an effective method could fabricate micro/nano structures directly on the material surface and to control the pattern of micro/nano structure accurately [6] [7]. Moreover, as a widely used preparation technology, laser fabricate has many advantages, including simple processing process, high preparation precision, wide processing materials, and complex structure of micro/nano preparation. The surface structure is usually stable after laser processed, which is very important to obtain the persistent micro/nano structure [6].

The purpose of this study is focused on the effect of the laser texturing process on the roughness, hydrophobicity and hydrophilicity of an aluminium surface using a fiber laser.

II. MATERIAL AND METHODS

2.1. Material

Aluminum is a soft, lightweight, silvery-white metal with high thermal and electrical conductivity. Melting point 660° C. Aluminum is widely used as a structural material. The main advantages of aluminum in this aspect are lightness, pliability to stamping, corrosion resistance (in air, aluminum is instantly covered with a strong film of Al_2O_3, which prevents its further oxidation), high thermal conductivity, and non-toxicity of its compounds. The main disadvantage of aluminum as a structural material is its low strength, so it is usually alloyed with a small amount of copper and magnesium (the alloy is called duralumin). In Table 1 physical properties of aluminium alloy 9995 are shown.

TABLE 1 PHYSICAL PROPERTIES OF ALUMINIUM 9995

Density, (kg / m^3)	2,7
Melting point T_m, ° C	660
Boiling point T_{boil}, ° C	2327
Latent heat of fusion, J/ g	393,6
Thermal conductivity l, W/ m × K (at 20 ° C)	228
Heat capacity Cp, J / (g × K) (at 0–100 ° C)	0,88
Linear expansion coefficient α × $10^{-6, 1}$ / ° C (pr ° C)	24,3
Electrical resistance ρ × 10-8, Ohm × m (at 20 ° C)	2,7
Ultimate strength σ in, MPa	40-60
Elongation δ, %	40-50
Brinell hardness HB	25
Normal elastic modulus E, GPa	70

2.2. Laser system

Within this study the nanosecond fiber laser Rofin Sinar GmbH system PowerLine f20 Varia was used to process aluminium samples within focal distance with the minimum spot size. Rofin PowerLine F20 Varia technical parameters could be observed in Table 2.

TABLE 2 ROFIN POWERLINE F20 VARIA TECHNICAL PARAMETERS

Sym-bol	Name	Value range	Step	Units
kp	Power regulation factor	0...1	0.001	N/A
f	Pulse repetition frequency	2..1000	0.001	kHz
v	Scan speed	1..20000	1	mm/s
Δx	Line step	0.001..120	0.001	mm
τ	Pulse duration	4, 8, 14, 20, 30, 50, 100, 200	-	ns
Δf	Focus shift	-10..10	-0.5	mm

Given nanosecond laser main system parameters could be observed in Table 3.

TABLE 3 ROFIN POWERLINE F20 VARIA SYSTEM PARAMETERS

Laser type	Diode pumped Yb fiber laser
Wavelength	1065 nm ± 5 nm
Repetition rate	Programmable
Impulse energy	0.95 mJ
Beam quality, M^2	<1.5
Focal spot size	40 µm

2.3. Microscopes

For measurements were used: 3D laser scanning microscope OLYMPUS LEXT OLS500 and a microscope Dino-Lite Premier AM7115MZT.

Roughness measurements and the resulting microstructure were examined with an Olympus model "OLS5100-EAF" laser microscope, see Fig.1. The obtained microstructural images were carried out using a 20× objective, magnification 451×, as the examined area for each measurement 1280×1280 µm with a measurement accuracy of ± 2.0 µm. From the obtained 3D images with the laser system of the microscope, the roughness Ra and Rz perpendicular to the marking lines with a length of 1280 µm, and the roughness Rq for the entire examined area 1280×1280 µm were measured. The obtained values are plotted in tables and graphical dependences of changes in roughness depending on speed and step during surface laser processing are shown. The built dependencies are presented in the results [9].

Fig.1. OLS5100-EAF" laser microscope [9].

Measurements with such laser scanning microsope gives the opportunity to observe produced structure on the surface of materials, example could be observed in Fig. 2.

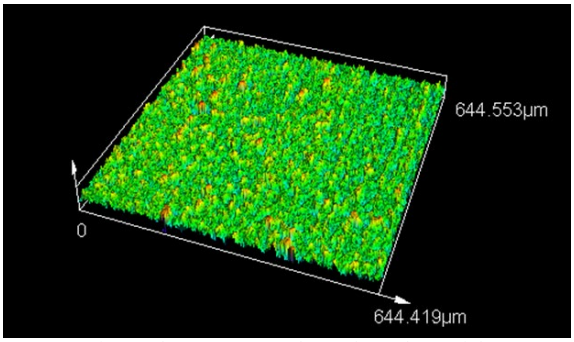

Fig. 2. The structure on the surface of material.

The Dino-Lite Premier AM7115MZT digital handheld microscope has a 5 Megapixels sensor with magnification up to 220x depending on working distance with a resolution of up to 2592x1944 [10].

Given digital handheld microscope could be observed in Fig.3.

Fig.3.The microscope Dino-Lite Premier AM7115MZT [11]

Using a Dino-Lite Premier AM7115MZT microscope and DinoCapture 2.0 software, measurements were made with the magnification 1x mode to determine the hydrophobic and hydrophilic properties of the aluminium surface ASTM D7334-08 (2022) [11]. Example of made measurements could be observed in fig. 4.

Fig.4.The measurement of the contact angle.

2.3. Applied laser parameters

Using the Rofin PowerLine F20 fiber laser, 2 matrixes were made on aluminium alloy. Each matrix consisted of 8 columns and 5 rows thus forming a rectangle with 40 squeres inside. In the first matrix, the constant parameters were the power regulation coeficient P = 10%; frequency f= 25 kHz; and pulse duration τ =30 ns. In the second matrix, the constant parameters were the marking speed v = 50 mm/s; pulse duration τ = 30 ns; and frequency f = 25 kHz.

2.4. Equations

According to the formula there were made calculations to determine marking lines overlap ratio [13]:

$$Ksoc = 1 - \frac{\Delta x}{d} * 100\ \% \qquad (1)$$

Where:
Δx – marking line step;
d – laser focal spot size.

Laser surface structuring using a line-wise scanning strategy leads to a defined laser scanning line overlap (*Ksoc*) which very well describe formation of periodic ripples on aluminium surfaces which lead to establish corelations of roughness and contact angle.

III Results And Discussions

3.1. Measurement results of the Roughness on the surface.

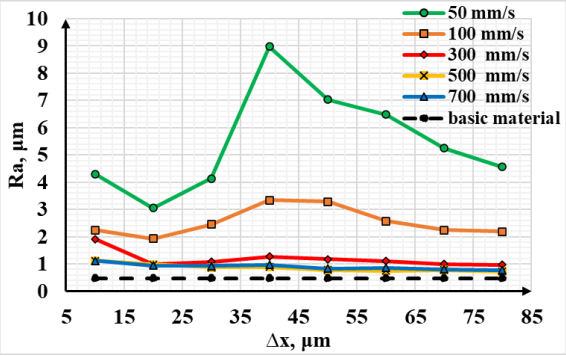

Fig.5. Dependence of the roughness *Ra* on the marking line step for the first matrix.

Data plotted for dependence of the roughness *Ra* on the marking line step could be observed in Fig.5. At a low-speed v = 50 mm/s, the roughness changes with the following trend: from 10 µm to 20 µm, the roughness decreases. From 20 to 40 µm, the roughness increases, and the maximum roughness value is obtained. The main reason for changes in roughness is their change in the overlap coefficient between lines. At 40 µm, the overlap factor is 0. With an increase from 40 µm to 80 µm, the overlap coefficient becomes negative and the roughness decreases. This trend of roughness changes also occurs with v = 100 mm/s, but with minor changes. And at a speed v = 300 mm/s at the beginning with a small delta X = 10 µm the roughness was maximum. With an increase in delta X by 20 µm, the roughness decreases. From 20 µm to 40 µm, the roughness increases in the range from 40 µm to 85 µm, the roughness *Ra* decreases. At the speed v = 500mm/s from 10 µm, the trend of *Ra* goes down.

And the same trend occurs at v = 700 mm/s.

Data plotted for dependence of roughness on velocity v with different marking line step could be observed in Fig.6. and it shows that roughness decreases with increasing speed. At the lowest speed, roughness decreases. At the initial roughness without marking, roughness was relatively small. Roughness *Ra* increased in the range from 1.5 to 10.95 times, thus at v=50 mm/s roughness was the highest. In the speed range from 550 mm/s to 750 mm/s, the roughness was similar.

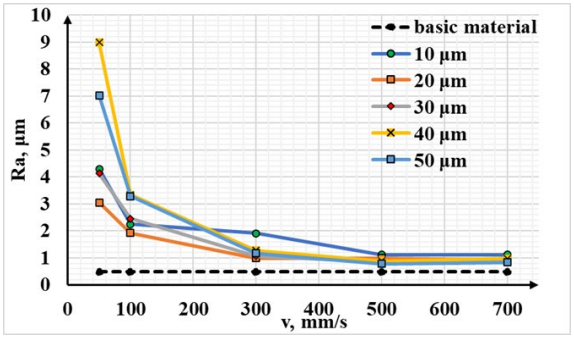

Fig.6. Dependence of roughness on velocity *v*, mm/s for the first matrix.

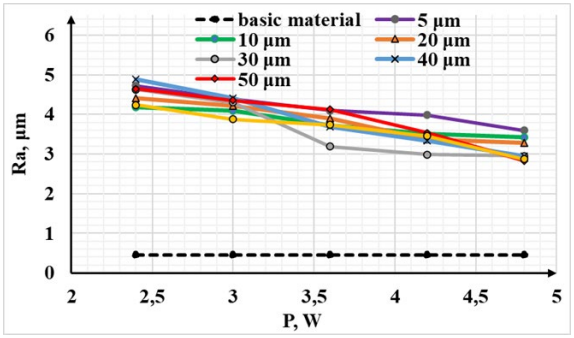

Fig.7. Dependence of roughness *Ra* on power *P*, W.

Data plotted for dependence of roughness Ra on power *P* with different marking line step factors could be observed in Fig.7.

With a small step of 5 µm and a small power P = 2.4 W, the surface changes and a new chaotic structure is obtained. With a step of 5 µm and an increase in power from 3.6 W to 4.8 W, droplets are formed, which prove a decrease in roughness. In the 10 µm range, there was a transition from evaporation to melting, in which there was a decrease in roughness. At 20 µm, the transition zone has changed at a high power of 3.6 W and the roughness has decreased. With a step of 30-50 µm, *Ra* increases at a power of 2.4 W.

At 50 µm, the overlap coefficient is negative between the lines and roughness *Ra* will be high. As the power *P* increases, the effects on the impact of the laser spot increase. As the power *P* increases, melting also occurs between the lines.

At the maximum value of 70 µm, the line spacing is high and the power *P* energy at 2.4 W will result in energy reflection and little melting. As the power *P* increases, the roughness *Ra* changes with a small difference.

Data plotted for dependence of the roughness *Ra* on the marking line step with different power factors could be observed in Fig.8.

At a power of 2.4 W, the roughness *Ra* was the highest. The main reason for the high roughness *Ra* is the impact on the surface, which results in deep channels.

With an increase in power *P* by 3.0 W, the roughness *Ra* decreases. At power P = 3.6 W, a transition zone between evaporation and melting is obtained.

At a power of *P* 4.2-4.8, the main melting occurs on the surface and the roughness *Ra* decreases.

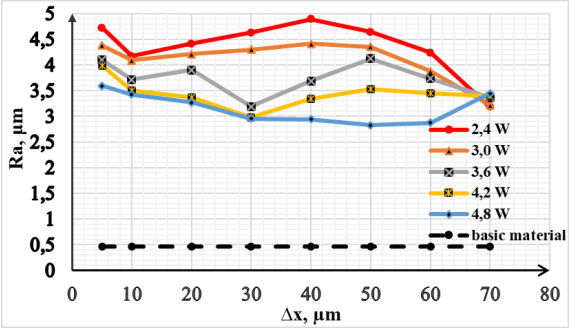

Fig.8. Dependence of the roughness *Ra* on the marking line step for the second matrix.

3.3. Measurement results of the hydrophobicity and hydrophilicity.

Data plotted for *CA* dependence on the line marking step with different speed factors could be observed in Fig.9.

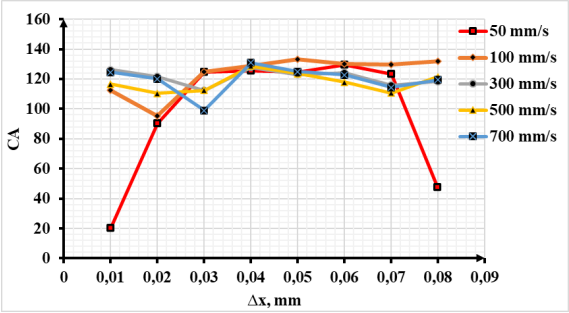

Fig.9. Dependence of the contact angle on delta x for the first matrix.

At a low speed of 50 mm/s, the droplets change depending on the pitch.

With a small step, the angle of the drop is about 20 degrees, that is, hydrophilic. The main reason is the high coefficient of spot overlap and the structure on the surface is obtained with a small roughness.

As the pitch increases to 40 µm, the roughness increases. The overlap factor between lines is reduced. And the maximum hydrophobicity is obtained at a step of 40 µm. And this structure changes from hydrophilic to hydrophobic.

With an increase in pitch from 40 µm to 80 µm the structure on the surface turns from hydrophobic to hydrophilic. At a speed of 100 mm/s and with a small step delta X, a transition zone between hydrophilic and hydrophobic is obtained on the surface structure.

An angle of about 130 degrees is achieved.

At a speed of 300-500 mm/s with a small step from 0.01 to 0.04 the surface becomes more hydrophobic. And the maximum hydrophobicity is obtained at a step of 40 µm. From 40 to 80 µm per surface structure, a decrease in hydrophobicity is obtained. At a maximum speed of 700 mm/s, the initial hydrophobicity is high. With an increase in pitch by 30 µm, which leads to a decrease in hydrophobicity properties. At 40 on the surface is obtained.

From 40 µm to 80 µm, a change in the surface of the structure results in a smooth transient decrease in hydrophobicity. The surface structure is retained by hydrophobic compared to the speed of 50 mm/s has changed to hydrophilic.

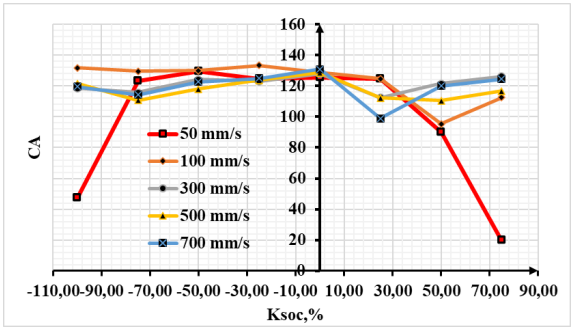

Fig.10. dependence of the contact angle on Ksoc for the first matrix.

The graph shows changes in the angle of the drop depending on the overlap coefficient. With a small overlap ratio and a low speed of 50 mm.s, the surface changes are hydrophilic. With an increase in the overlap coefficient from -40 to 25, the surface structure becomes hydrophobic. Above 25 the overlap ratio the surface changes from hydrophobic to hydrophilic. At high speeds from 100-700 mm/s, the overlap ratio indicates little change in hydrophobicity.

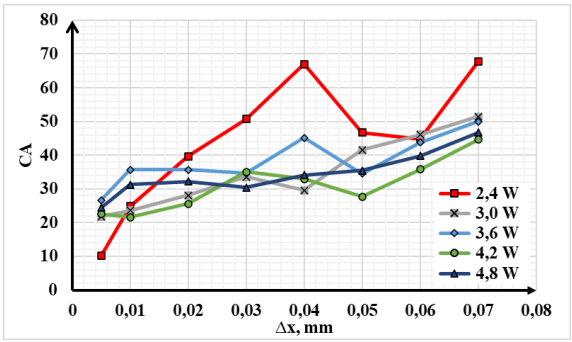

Fig.11. Dependence of the contact angle on delta x for the second matrix.

With a step of power surface treatment from 2.4 to 4.8 W, the surface structure will change from high hydrophilicity to low hydrophilicity.

At a power of 2.4 W, the changes are on the surface with the highest trend.

With a small step, the hydrophilicity is the highest. With an increase in delta X to 40 µm, the hydrophilicity decreases. With an increase in pitch from 40 µm to 60, the surface structure becomes hydrophilic. Above 60 µm a decrease in hydrophilicity is obtained.

At a power of 3.0 and 4.2 W from 10 µm to 30 µm, the hydrophilicity decreases.

The surface structure creates conditions for reducing hydrophilicity.

In a trend from 10 to 40 µm, hydrophilicity changes poorly.

As the pitch increases from 50 µm to 70 µm, the hydrophilicity decreases.

At 3.6 W, the hydrophilicity decreases with a small step from 10 to 40 µm, since the contact angle of the drop increases and the hydrophilicity decreases. In the range from 40 to 50 µm, a transition zone is obtained - the drop angle decreases and the hydrophilicity increases. From 50 to 70 µm the surface structure changes and the hydrophilicity decreases. With a maximum power of 4.8 W from 10 µm to 70 µm, the surface will gradually change to a slight hydrophilicity. This processing regime creates conditions for hydrophilicity, but not for hydrophobicity.

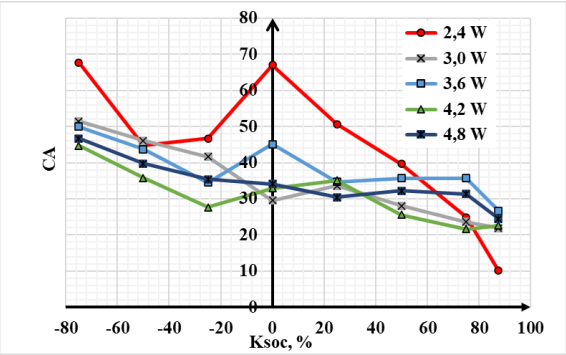

Fig.12. Dependence of the contact angle on Ksoc for the second matrix.

The overlap ratio indicates the effects of surface texture on hydrophilicity. At a low power of 2.4 W and a small *Ksoc* of -80 to -60, the surface texture indicates an improvement in hydrophilicity.

From -60 to 0 *Ksoc* the hydrophilicity decreases, the drop angle increases, and minimal hydrophilicity is obtained.

From 0 to 80 *Ksoc* creates conditions for improving hydrophilicity.

From 3.0 to 4.8 W, an overlap factor between lines from -80 to 90 indicates the effect of increasing hydrophilicity.

IV Conclusion

Low speed (v = 50 mm/s) resulted in an initial decrease in roughness (Ra) from 10 to 20 µm, followed by an increase to a maximum at 20 to 40 µm, attributed to the overlap coefficient between lines. Beyond 40 µm, the overlap coefficient becomes negative, resulting in a decrease in roughness as the marking line step increases to 80 µm. Similar trends were observed at v = 100 mm/s. At v = 300 mm/s, Ra reaches a maximum at 10 µm marking line step, then decreases with an increase in delta X by 20 µm. Roughness increases from 20 to 40 µm, but decreases again from 40 to 85 µm. At higher speeds (v = 500 mm/s and v = 700 mm/s), the trend of decreasing roughness with increasing marking line step is also observed.

Ra increased in the range from 1.5 to 10.95 times at the lowest speed (v = 50 mm/s), with the highest roughness observed at this speed. In the speed range from 550 mm/s to 750 mm/s, the roughness remained similar.

Small line step of 5 µm and low power of P = 2.4 W resulted in changes in surface structure, with a new chaotic structure observed. With an increase in power from 3.6 W to 4.8 W, droplets are formed, indicating a decrease in roughness. A transition from evaporation to melting is observed at 10 µm, resulting in a decrease in roughness. At 20 µm, the transition zone changes at a high power of 3.6 W, resulting in a decrease in roughness. On the other hand, with a step of 30-50 µm, roughness Ra increases at a power of 2.4 W. At 50 µm, the overlap coefficient between lines becomes negative, resulting in higher roughness Ra. As the power P increases, the effects of the laser spot impact and melting between lines also increase.

At the maximum line step of 70 µm, the energy from power P of 2.4 W is reflected with little melting, and roughness Ra changes with small differences as the power P increases.

Power factor (P) plays a significant role in the surface morphology and roughness of the marked area, with higher power levels generally resulting in lower roughness values. At a power of 2.4 W, the roughness Ra was found to be the highest, which can be attributed to the impact of the laser on the surface, resulting in deep channels and increased roughness. However, with an increase in power P to 3.0 W, the roughness Ra decreases. At a power of 3.6 W, a transition zone between evaporation and melting is observed, which affects the roughness Ra. At power levels of 4.2-4.8 W, the main melting occurs on the surface, leading to a decrease in roughness Ra.

At a low speed of 50 mm/s, the pitch between lines affects the hydrophobicity of the surface. A small pitch results in a hydrophilic surface with an angle of about 20 degrees, due to high spot overlap and small surface roughness. As the pitch increases to 40 µm, the roughness increases, reducing the overlap factor and achieving maximum hydrophobicity. Further increase in pitch to 80 µm changes the surface structure and increases the hydrophilicity of the surface. This is because at higher pitch values, the surface texture becomes more regular and the microstructures are spaced further apart, allowing for more water to fill in the gaps and wet the surface.

In addition to pitch, other factors such as the depth and shape of the microstructures can also affect the hydrophobicity or hydrophilicity of a surface. For example, deeper microstructures with sharp edges can create air pockets that repel water, resulting in increased hydrophobicity. On the other hand, shallower or rounded microstructures can allow for more water to penetrate and wet the surface, leading to increased hydrophilicity.

Surface roughness is another important parameter that can influence hydrophobicity or hydrophilicity. Rougher surfaces with irregular features tend to be more hydrophobic as they trap air and reduce the contact area between water and the surface. In contrast, smoother surfaces with less roughness tend to be more hydrophilic as they allow for more intimate contact between water molecules and the surface.

The hydrophobic or hydrophilic nature of a surface can have important practical applications in various fields,

including materials science, coatings, and biomedical engineering. For example, hydrophobic surfaces can be used to repel water and prevent fouling, icing, or corrosion, while hydrophilic surfaces can be used to promote wetting and adhesion, enhance heat transfer, or facilitate biological processes.

In summary, the pitch, depth, shape, and roughness of microstructures on a surface can all influence its hydrophobicity or hydrophilicity. Understanding these parameters and their effects on surface properties is crucial for designing functional surfaces with tailored wetting behaviour for specific applications.

ACKNOWLEDGMENT

This work was developed within the framework of Latvian Postdoctoral Research Support Program "Analysis of new industrial materials laser marking process parameters for high-tech applications" No. 1.1.1.2/VIAA/3/19/474

REFERENCES

[1] Pang, Xiaobing & Dai, Jiahui & Chen, Shun & Zhang, Mingjun. (2019). Microstructure and Mechanical Properties of Fiber Laser Welding of Aluminum Alloy with Beam Oscillation. Applied Sciences. 9. 5096. 10.3390/app9235096.

[2] Suker, Dhia & Alsoufi, Mohammad & Alhusaini, Majdi & Azam, Sufyan. (2016). Studying the Effect of Cutting Conditions in Turning Process on Surface Roughness for Different Materials. World Journal of Research and Review (WJRR). 2. 16-21.

[3] Zaifuddin, Amira & Aiman, M & Quazi, M & Ishak, Mahadzir & Shamini, J. (2021). Influence of Laser Surface Texturing (LST) Parameters on the Surface Characteristics of Ti6Al4V and the Effects Thereof on Laser Heating. Lasers in Engineering. 355-367.

[4] Moldovan, Edit & Doria, Carlos & Ocaña, José L. & Baltes, Liana & Elena-Manuela, Stanciu & Croitoru, Catalin & Alexandru, Pascu & Roata, Ionut & Tierean, Mircea. (2022). Wettability and Surface Roughness Analysis of Laser Surface Texturing of AISI 430 Stainless Steel. Materials. 15. 2955. 10.3390/ma15082955.

[5] Przestacki, Damian & Jankowiak, M. (2014). Surface roughness analysis after laser assisted machining of hard to cut materials. Journal of Physics: Conference Series. 483. 012019. 10.1088/1742-6596/483/1/012019.

[6] Zhao, Jingnan & Guo, Jian & Shrotriya, Pranav & Wang, Yan & Han, Yinfeng & Dong, Yinghuai & Yang, Shuo. (2019). A rapid one-step nanosecond laser process for fabrication of super-hydrophilic aluminum surface. Optics & Laser Technology. 117. 134-141. 10.1016/j.optlastec.2019.04.015.

[7] Guo, Jian & Ma, Xiaolei & Si, Xuekang & Yang, Zeng & Zhao, Jingnan. (2019). Effect of Nanosecond Laser Treatment Parameters on Surface Wettability Behaviour of Pure Aluminium. IOP Conference Series: Materials Science and Engineering. 538. 012021. 10.1088/1757-899X/538/1/012021.

[8] Research Of Possibilities Of Laser Polishing Of The Surface Of Aluminum, Author: Kevins Bulavskis, Imants Adijāns, e-mail: k26bulavskis@gmail.com; Scientific supervisor: Lyubomir Lazov, Prof., Dr.sc.ing.,Rezekne Academy of technologies

[9] Olympus Global Homepage [ONLINE], 28.March 2023 AVALAIBLE: https://www.olympus-global.com/news/2017/nr00633.html

[10] Dino-lite microscope homepage [0NLINE], 28.March 2023 AVALAIBLE: https://www.dino-lite.com/products_detail.php?index_m1_id=9&index_m2_id=0&index_id=53

[11] Standard Practice for Surface Wettability of Coatings, Substrates and Pigments ASTM D7334-08 (2022) standard.

by Advancing Contact Angle Measurement1.

[12] Farayibi, P. K. & Akisin, Cletus & Ijaola, Ahmed. (2020). Wettability Transition for Laser Textured Surfaces: A Comprehensive Review.

[13] Schnell, Georg & Duenow, Ulrike & Seitz, Hermann. (2020). Effect of Laser Pulse Overlap and Scanning Line Overlap on Femtosecond Laser-Structured Ti6Al4V Surfaces. Materials. 13. 969. 10.3390/ma13040969.